X-ray Investigations of Liquid Bismuth-Copper Alloys

J. Nomssi Nzali and W. Hoyer

Institut für Physik, Technical University Chemnitz, D-09107 Chemnitz

Reprint requests to Prof. W. H.; Fax: +49 371 531 3555; E-mail: hoyer@physik.tu-chemnitz.de

Z. Naturforsch. **55 a,** 381–389 (2000); received May 29, 1999

Liquid copper, bismuth, and eleven bismuth-copper alloys were investigated at temperatures above the liquidus with X-ray diffraction. The experimental procedure was adjusted to reduce the effects of evaporation. The Faber-Ziman total structure factors $S(Q)$ feature a splitting of the first maximum and negative values for Q around 1 $Å^{-1}$ in a large concentration range. The results are compared to previous neutron diffraction results by Zaiss and Steeb, to square-well potential model calculations by Gopala Rao and Satpathy and to a simple segregation model. The segregation model reproduces the features qualitatively. Partial structure factors are assessed by fitting both neutron and X-ray scattering results with reverse Monte-Carlo simulation.

Key words: Bismuth; Copper; Liquid Alloys; X-ray Diffraction; Microsegregation.

1. Introduction

Liquid Bi-Cu alloys are miscible in all proportions, the Bi-Cu phase diagram is of the eutectic type (Fig. 1), with the eutectic point very close to pure Bi. The inflexion point in the liquidus line hints at a change of the short range order. The large difference of the atomic volumes and the small difference in electronegativity led Chang et al. [1] to use a self-associate model [2] to fit the liquidus line. From it, they suggest that the most stable associate configurations in liquid Bi-Cu alloys are Bi_7 and Cu_5 and they predict a metastable liquid miscibility gap with a critical point at 37.7 at.% Bi, 674.8 °C. Gopala Rao and Satpathy [3] assessed Bi-Cu partial structure factors by fitting the total structure factors from neutron scattering by Zaiss and Steeb [4], using the square well pair potential. Our work presents X-ray diffraction investigations of liquid Bi-Cu alloys, compares the results to the neutron scattering results and discusses the results in terms of a simple segregation and a square-well potential model. A refined set of partial structure factors is evaluated using a reverse Monte-Carlo simulation technique.

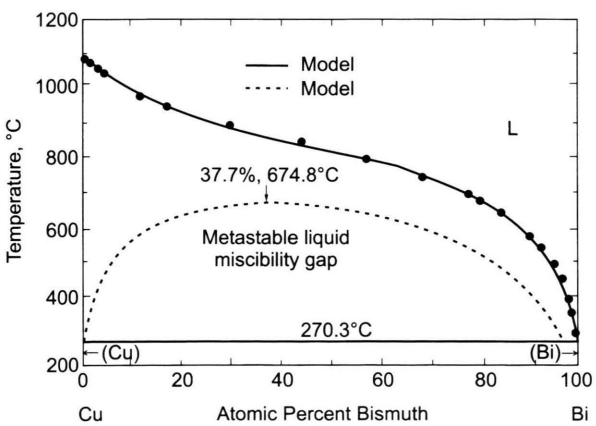

Fig. 1. The Cu-Bi phase diagram with the metastable miscibility gap in the liquid state [1].

2. X-Ray Wide-angle Scattering from Liquid Alloys

The intensity curve from the scattering of an incident X-ray beam by electrons in the atomic shells of a liquid alloy is recorded as $I(Q)$, where $Q = 4\pi \sin\theta/\lambda$ is the momentum transfer, 2θ the scattering angle and λ the wavelength of the X-ray beam. $I(Q)$ is corrected for background, polarisation, and absorption [5], and then normalised [6]. The incoherent scattering [7] is subtracted to extract the coherently scattered intensity per atom $I_a^{coh}(Q)$. The Faber-Ziman total structure factor $S(Q)$ is then calculated as

$$S(Q) = \frac{I_a^{coh}(Q) - \left\{\langle f^2(Q)\rangle - \langle f(Q)\rangle^2\right\}}{\langle f(Q)\rangle^2} \quad (1)$$

0932–0784 / 00 / 0300–0381 $ 06.00

with

$$\langle f^2(Q)\rangle = \sum_j c_j f_j^2(Q),\ \langle f(Q)\rangle = \sum_j c_j f_j(Q). \quad (2)$$

c_j is the mole fraction and $f_j = f_j^0 + f_j' + if_j''$ the total atomic scattering factor of the j-th component in the alloy. A linear combination of four Gaussians [8] is used to fit the electron density term f_j^0. The anomalous dispersion terms f_j' and f_j'' are computed as in [9, 10]. In the Faber-Ziman formalism [11], the total structure factor of the binary Bi-Cu alloy is the weighted sum of the three partial structure factors $S_{\mathrm{BiBi}}(Q)$, $S_{\mathrm{CuCu}}(Q)$ and $S_{\mathrm{BiCu}}(Q)$:

$$S(Q) = w_{\mathrm{BiBi}} S_{\mathrm{BiBi}}(Q) + w_{\mathrm{BiCu}} S_{\mathrm{BiCu}}(Q) + w_{\mathrm{CuCu}} S_{\mathrm{CuCu}}(Q). \quad (3)$$

The weight factors for X-ray scattering are

$$w_{\mathrm{BiBi}}^{\mathrm{X}} = \frac{c_{\mathrm{Bi}}^2 f_{\mathrm{Bi}}^2(Q)}{\langle f(Q)\rangle^2}, \quad (4)$$

$$w_{\mathrm{CuCu}}^{\mathrm{X}} = \frac{c_{\mathrm{Cu}}^2 f_{\mathrm{Cu}}^2(Q)}{\langle f(Q)\rangle^2}, \quad (5)$$

$$w_{\mathrm{BiCu}}^{\mathrm{X}} = \frac{2c_{\mathrm{Bi}}c_{\mathrm{Cu}} f_{\mathrm{Bi}}(Q) f_{\mathrm{Cu}}(Q)}{\langle f(Q)\rangle^2}. \quad (6)$$

The total pair correlation function $g(r)$ is obtained via the transformation

$$g(r) = \frac{\rho(r)}{\rho_0} = 1 + \frac{1}{2\pi^2 r \rho_0}\int_0^\infty Q\,(S(Q) - 1)\sin(Q \cdot r)\,\mathrm{d}Q, \quad (7)$$

where $\rho(r)$ and ρ_0 are the local and average number density, respectively. The average number densities ρ_0 needed for the Bi-Cu alloys were taken or interpolated from [12]. The position of the first maximum of $g(r)$ is the mean nearest neighbour distance r^I. The coordination number

$$N = \int_{r_1}^{r_2} 4\pi r^2 \rho_0 g(r)\,\mathrm{d}r \quad (8)$$

is the mean number of nearest neighbours, r_1 and r_2 denote the lower and upper limit of the first maximum of $4\pi r^2 \rho_0 g(r)$.

3. Experimental Procedure

3.1. X-ray Scattering Apparatus

The scattering apparatus consists of a θ-θ goniometer with Bragg-Brentano focussing. The sample is fixed on the horizontal axis, the X-ray source and the counting system rotate in equal steps in opposite directions. A focussing graphite monochromator installed in the diffracted beam selects the MoK_α wavelength of $\lambda = 0.71069$ Å. The scattered intensity is measured with a scintillation detector with pulse height analyser. The available angular range converts into a largest momentum transfer of $Q = 12$ Å^{-1}. A calibration of the Q scale with a silicon powder sample shows a deviation less than 0.025 Å^{-1}. The intensity is recorded in steps of 0.05 Å^{-1} for $Q \leq 5$ Å^{-1} and in steps of 0.1 Å^{-1} for $Q > 5$ Å^{-1}.

3.2. Vacuum Chamber and Furnace

The water-cooled vacuum chamber contains a furnace for temperatures up to 1200 °C. The furnace's thermal shield and the chamber have beryllium windows for the incident and scattered X-ray beams. All samples are prepared by melting from granules with 99.99 at.% of the pure materials. The rectangular graphite crucible has the internal dimensions of $(24 \times 39)\mathrm{mm}^2 \times 2\mathrm{mm}$ depth and a special bore fit for the NiCr-Ni-thermocouple. A regulator maintains the sample temperature within 1 K of the set point during a measurement. A calibration of the sample temperature at the melting points of pure Bi, Pb, Sb, and Ag yielded absolute differences of less than 1 K at 327 °C and 3 K at 962 °C. As the furnace's tungsten winding and the thermocouple were replaced often, the accuracy of the temperature is more likely around 1%. The whole furnace is moved vertically from outside the chamber to adjust the sample height before a measurement.

3.3. Experimental Details

The chamber is evacuated to about 10^{-4} mbar and filled with a gas mixture of 90% Ar and 10% H_2 in the 500 mbar range. The reactive gas H_2 effectively reduces the Bi-oxide layer on the sample surface at temperatures above 900 °C [13]. Bi is regarded as the sole volatile component since its vapour pressure is 1.3 mbar at 934 °C while the vapour pressure of Cu is $1.3 \cdot 10^{-3}$ mbar at 1141 °C. Bi vaporises and condenses

Table 1. List of investigated samples with weight factors for X-ray and neutron scattering and a figure of merit R [18].

Sample (at.%)	Temperature (°C)	w^{X}_{CuCu}	w^{X}_{BiBi}	w^{X}_{BiCu}	w^{n}_{CuCu}	w^{n}_{BiBi}	w^{n}_{BiCu}	R
Cu ($Z = 29$)	1088	1.000	0.000	0.000	1.000	0.000	0.000	–
$Cu_{90}Bi_{10}$	1050	0.576	0.058	0.366	0.793	0.012	0.195	0.40
$Cu_{80}Bi_{20}$	980	0.340	0.174	0.486	0.614	0.047	0.339	0.44
$Cu_{70}Bi_{30}$	950	0.202	0.303	0.495	0.460	0.103	0.437	0.45
$Cu_{62}Bi_{38}$	900	0.132	0.406	0.462	0.355	0.163	0.482	0.45
$Cu_{55}Bi_{45}$	860	0.090	0.491	0.419	0.276	0.225	0.499	0.45
$Cu_{50}Bi_{50}$	870	0.067	0.559	0.384	0.225	0.276	0.499	0.44
$Cu_{45}Bi_{55}$	870	0.050	0.605	0.346	0.181	0.330	0.489	0.44
$Cu_{40}Bi_{60}$	850	0.036	0.658	0.306	0.142	0.389	0.469	0.43
$Cu_{30}Bi_{70}$	780	0.017	0.756	0.227	0.078	0.519	0.403	0.41
$Cu_{20}Bi_{80}$	750	0.006	0.846	0.148	0.034	0.665	0.301	0.39
$Cu_{10}Bi_{90}$	612	0.001	0.927	0.072	0.008	0.826	0.166	0.36
Bi ($Z = 83$)	300, 475, 600, 700, 900	0.000	1.000	0.000	0.000	1.000	0.000	–

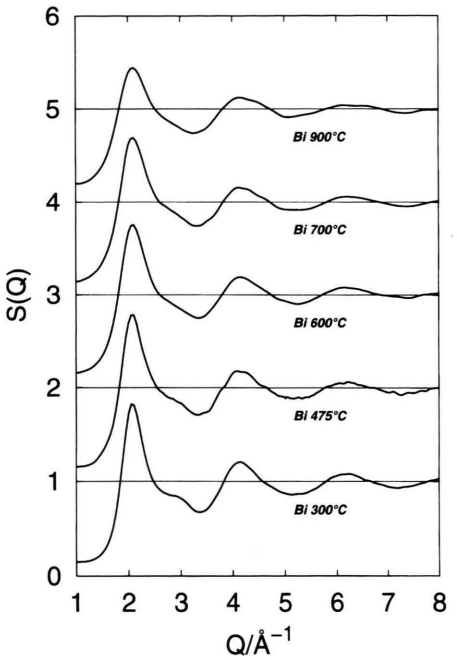

Fig. 2. Bi-structure factors, temperature dependence.

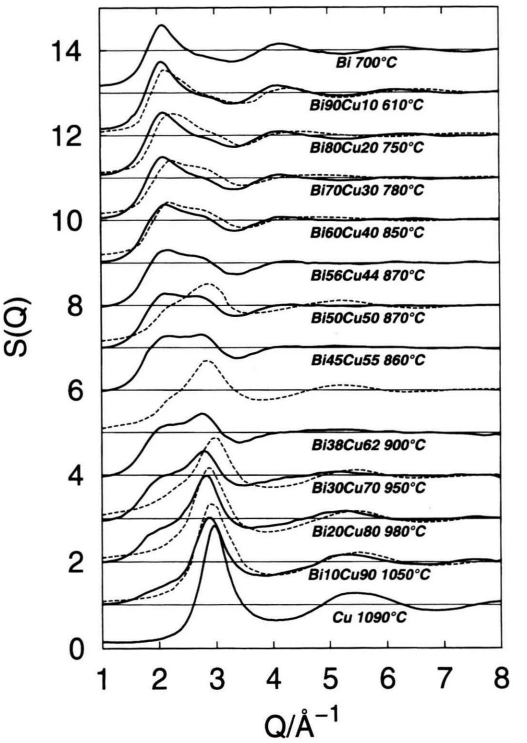

Fig. 3. Bi-Cu total Faber-Ziman structure factors; full line: this work, dashed line: neutron measurements from [4].

as a thin film on the walls of the chamber, the sample concentration varies during the measurement and the X-ray beam passing through the beryllium windows might be attenuated. The thin Bi-film on the beryllium windows is removed after each run. The length of a measurement run was abridged by reducing the relative accuracy of the count rate (better than 3.5%) and repeating runs. Most structure factors were measured from 1 Å^{-1} up to 10 Å^{-1} or 8 Å^{-1} only. The mass loss of the sample was recorded after each run and compensated with Bi granules. With this, fluctuations of the sample concentration were kept below 1 at.%.

4. Results

4.1. Structure Factors

Table 1 lists the investigated samples with the weight factors for X-ray and for neutron scattering. The latter are evaluated by substituting the coherent neutron scattering lengths [14] for the atomic scattering factors in (4 - 6). Liquid Bi was investigated

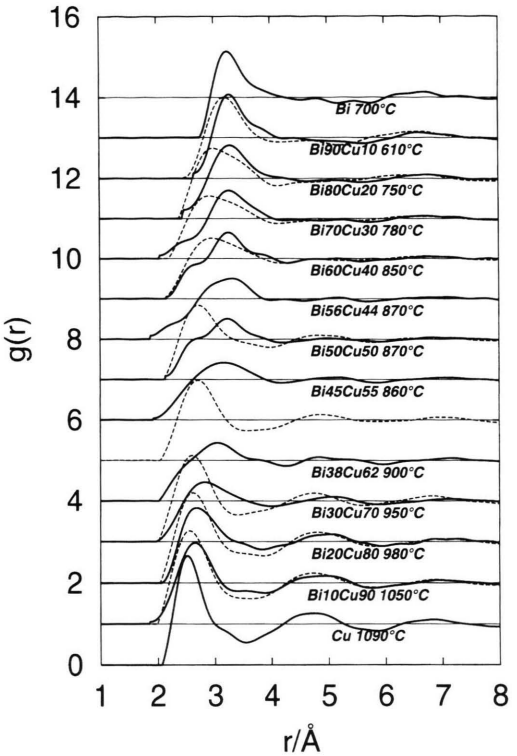

Fig. 4. Bi-Cu total pair correlation functions $g(r)$; *full* line: this work, *dashed* line: using neutron measurements from [4].

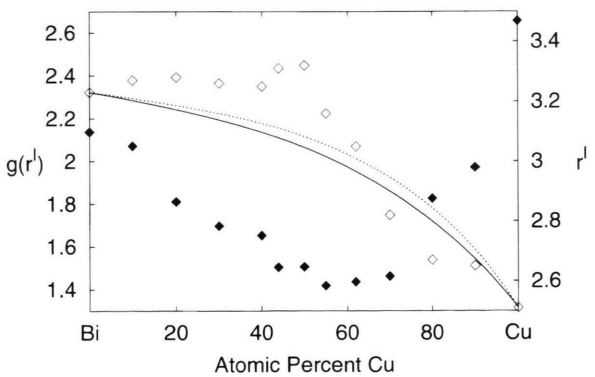

Fig. 5. Concentration dependence of first maximum of Bi-Cu $g(r)$; *empty* diamonds ◇: position of r^I of first maximum of $g(r)$; *filled* diamonds ◆: height $g(r^I)$ of first maximum; *full* line: statistical model for r^I; *dashed* line: demixing model for r^I.

between 250 °C and 900 °C, some structure factors $S(Q)$ are given in Figure 2. The total structure factors and pair correlation functions of the liquid Bi-Cu alloys are given in Figure 3. The structure factor curves from neutron scattering plotted in [4] were digitalised and added as a reference in Figure 3. The pair correlation functions were computed and added in Figure 4. A closest approach distance r_1 was empirically selected, and $g(r)$ was set to zero for $r < r_1$.

4.2. *Nearest Neighbour Distance and Coordination Number*

The concentration dependence of the mean nearest neighbour distance r^I is plotted in Fig. 5 together with results from a demixing and a statistical mixture model [6]. The models use mean values for the X-ray scattering factors, averaged over the experimental Q-range:

$$K_{\mathrm{Bi}} = \left\langle \frac{f_{\mathrm{Bi}}(Q)}{f_{\mathrm{e}}(Q)} \right\rangle \text{ and } K_{\mathrm{Cu}} = \left\langle \frac{f_{\mathrm{Cu}}(Q)}{f_{\mathrm{e}}(Q)} \right\rangle, \tag{9}$$

$$\text{with } f_{\mathrm{e}}(Q) = \frac{c_{\mathrm{Bi}} f_{\mathrm{Bi}}(Q) + c_{\mathrm{Cu}} f_{\mathrm{Cu}}(Q)}{c_{\mathrm{Bi}} Z_{\mathrm{Bi}} + c_{\mathrm{Cu}} Z_{\mathrm{Cu}}}. \tag{10}$$

Z_{Bi} and Z_{Cu} are the atomic numbers of the components. The expressions for r^I are, with $\langle K \rangle = c_{\mathrm{Bi}} K_{\mathrm{Bi}} + c_{\mathrm{Cu}} K_{\mathrm{Cu}}$, for demixing

$$r^I = \frac{c_{\mathrm{Bi}} K_{\mathrm{Bi}}^2 N_{\mathrm{Bi}} r_{\mathrm{Bi}}^I + c_{\mathrm{Cu}} K_{\mathrm{Cu}}^2 N_{\mathrm{Cu}} r_{\mathrm{Cu}}^I}{c_{\mathrm{Bi}} K_{\mathrm{Bi}}^2 N_{\mathrm{Bi}} + c_{\mathrm{Cu}} K_{\mathrm{Cu}}^2 N_{\mathrm{Cu}}} \tag{11}$$

and for statistical distribution:

$$r^I = \frac{c_{\mathrm{Bi}} K_{\mathrm{Bi}} r_{\mathrm{Bi}}^I + c_{\mathrm{Cu}} K_{\mathrm{Cu}} r_{\mathrm{Cu}}^I}{\langle K \rangle}. \tag{12}$$

The first maximum of $g(r)$ in Fig. 4 is very broad in a large concentration range, it shows a shoulder whose shape is not well resolved. This uncertainty in the limits of the first maximum renders coordination numbers unreliable.

4.3. *Demixing Model for $S(Q)$*

Assuming a complete separation of the components, the coherently scattered intensity from the binary Bi-Cu alloy $I_{\mathrm{BiCu}}^{\mathrm{coh}}(Q)$ is written as a sum using the structure factors of the pure elements [13]

$$\begin{aligned} I_{\mathrm{BiCu}}^{\mathrm{coh}}(Q) &= c_{\mathrm{Bi}} I_{\mathrm{Bi}}^{\mathrm{coh}}(Q) + c_{\mathrm{Cu}} I_{\mathrm{Cu}}^{\mathrm{coh}}(Q) \\ &= c_{\mathrm{Bi}} f_{\mathrm{Bi}}^2(Q) S_{\mathrm{Bi}}(Q) + c_{\mathrm{Cu}} f_{\mathrm{Cu}}^2(Q) S_{\mathrm{Cu}}(Q). \end{aligned} \tag{13}$$

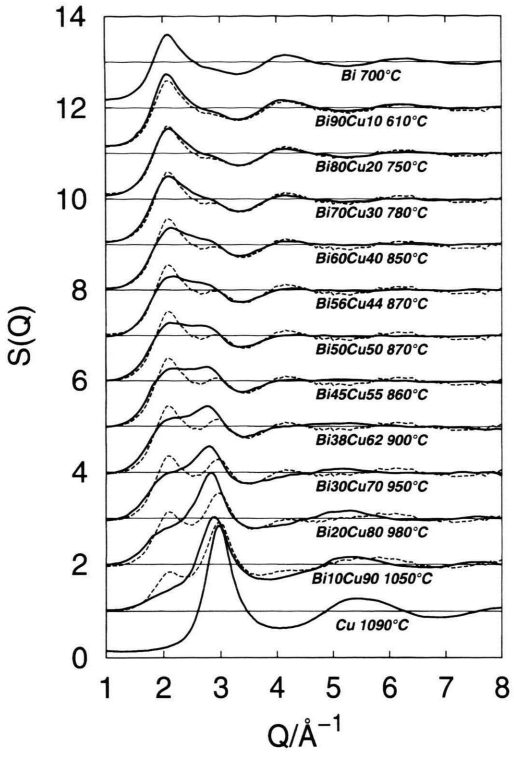

Fig. 6. Bi-Cu structure factors, comparison with a demixing model; *full* line: X-ray diffraction results; *dashed* line: demixing model.

With this, the total structure factor of the alloy is

$$S(Q) = \left[c_{\mathrm{Bi}} f_{\mathrm{Bi}}^2(Q) S_{\mathrm{Bi}}(Q) + c_{\mathrm{Cu}} f_{\mathrm{Cu}}^2(Q) S_{\mathrm{Cu}}(Q) - \left\{\langle f^2(Q)\rangle - \langle f(Q)\rangle^2\right\}\right] \Big/ \langle f(Q)\rangle^2. \quad (14)$$

The results are plotted in Figure 6. The model reproduces qualitatively the splitting of the first maximum, the growth of the shoulder on the left hand side and the course of $S(Q)$ in the Q-range with the negative values.

4.4. Square Well Potential Model

The analytical expressions for the partial structure factors of a mixture of hard spheres with an attractive tail (square well potential) in the Percus-Yevick approximation have been given in detail in [15, 16]. Gopala Rao and Satpathy [3] fitted the Bi-Cu total structure factors from neutron scattering [4] using the square well pair potential with a concentration dependence of the potential parameters. From those parameters (Table 2), the corresponding X-ray total structure factors were generated with (3) and compared to the experimental results in Figure 7. The model does not reproduce the splitting of the first maximum. Negative values of $S(Q)$ for the Q-range near 1 Å^{-1} are found, but the demixing model fits this Q-range better.

Table 2. Potential parameters used in the evaluation of partial structure factors of Bi-Cu melt, from [3].

Temp. °C	At.% of Cu	σ_{CuCu} (Å)	σ_{BiBi} (Å)	$\varepsilon_{\mathrm{CuCu}}/k_{\mathrm{B}}$ (K)	$\varepsilon_{\mathrm{BiBi}}/k_{\mathrm{B}}$ (K)	A_{CuCu}	A_{BiBi}
800	0.0	2.21	3.00	300	640	1.70	1.90
597	0.1	2.21	2.95	300	600	1.70	1.87
700	0.2	2.21	2.86	300	660	1.70	1.88
762	0.3	2.22	2.67	300	640	1.70	1.90
807	0.4	2.21	2.60	300	640	1.75	1.90
847	0.5	2.21	2.70	300	660	1.70	1.95
887	0.6	2.28	2.80	300	640	1.65	1.92
917	0.7	2.24	3.03	300	590	1.64	1.90
927	0.8	2.26	3.08	300	590	1.60	1.90
1002	0.9	2.22	3.00	300	640	1.70	1.95
1100	1.0	2.22	3.00	300	640	1.70	1.90

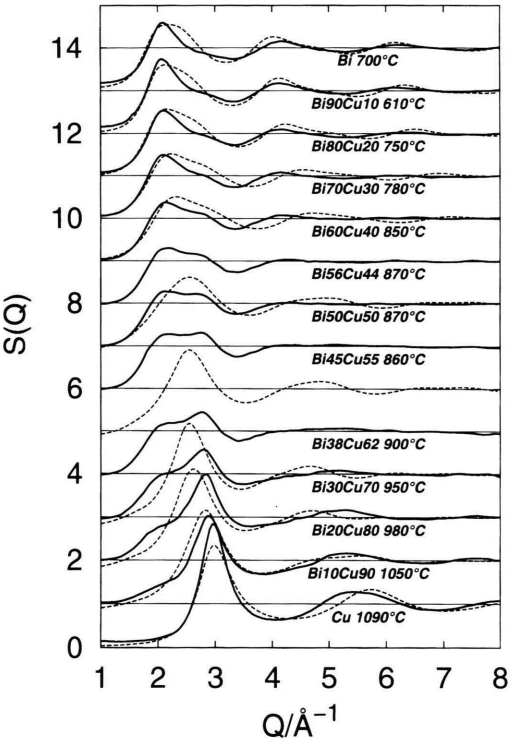

Fig. 7. Bi-Cu structure factors, comparison with the square well model; *full* line: X-ray diffraction results; *dashed* line: square-well potential calculations.

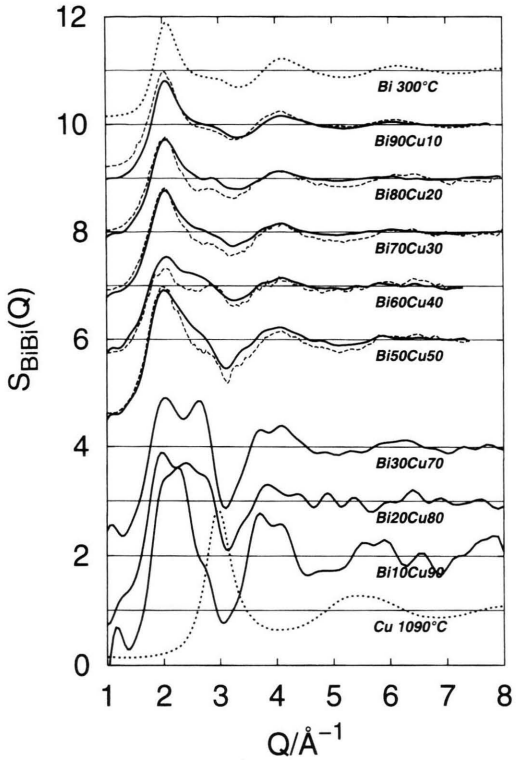

Fig. 8. Assessed partial Bi-Bi structure factors; *full* line: RMC simulation results; *dashed* line: approximation in Sect. 4.5, Eq. (15), (16); *dotted* line: pure elements.

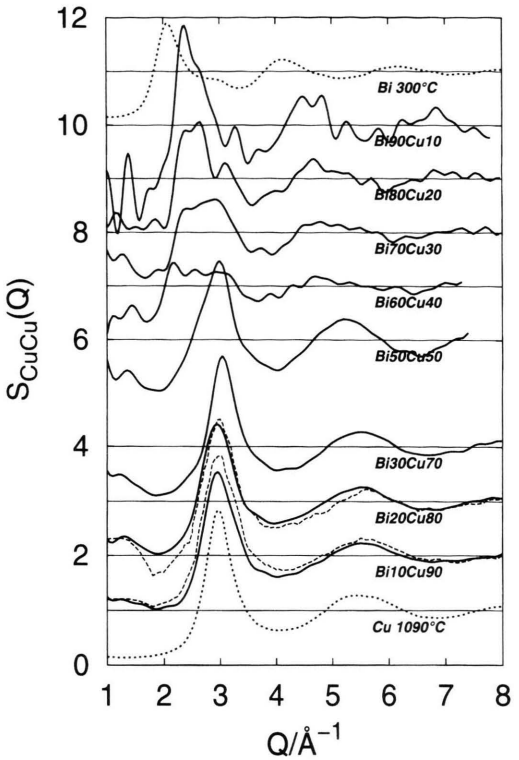

Fig. 9. Assessed partial Cu-Cu structure factors; *full* line: RMC simulation results; *dashed* line: approximation in Sect. 4.5, Eq. (17), (18); *dotted* line: pure elements.

4.5. Partial Structure Factors

The present results $S^{\mathrm{X}}(Q)$, combined with the neutron scattering results $S^{\mathrm{n}}(Q)$ from [4], give two independent equations (3) for the three partial structure factors $S_{\mathrm{BiCu}}(Q)$, $S_{\mathrm{BiBi}}(Q)$, and $S_{\mathrm{CuCu}}(Q)$. Approximations for $S_{\mathrm{BiCu}}(Q)$ and $S_{\mathrm{BiBi}}(Q)$ are obtained by replacing the partial structure factor $S_{\mathrm{CuCu}}(Q)$ for the Cu-Cu interaction by the structure factor $S_{\mathrm{Cu}}(Q)$ of pure Cu:

$$S^{\mathrm{X}}(Q) - w^{\mathrm{X}}_{\mathrm{CuCu}} S_{\mathrm{Cu}}(Q) \approx w^{\mathrm{X}}_{\mathrm{BiBi}} S_{\mathrm{BiBi}}(Q), \qquad (15)$$
$$+ w^{\mathrm{X}}_{\mathrm{BiCu}} S_{\mathrm{BiCu}}(Q)$$

$$S^{\mathrm{n}}(Q) - w^{\mathrm{n}}_{\mathrm{CuCu}} S_{\mathrm{Cu}}(Q) \approx w^{\mathrm{n}}_{\mathrm{BiBi}} S_{\mathrm{BiBi}}(Q), \qquad (16)$$
$$+ w^{\mathrm{n}}_{\mathrm{BiCu}} S_{\mathrm{BiCu}}(Q)$$

This approach yields better results for compositions near pure Bi, where the contribution of $S_{\mathrm{CuCu}}(Q)$ is weak (Table 1) and even a crude approximation of $S_{\mathrm{CuCu}}(Q)$ becomes acceptable. A similar procedure yields $S_{\mathrm{BiCu}}(Q)$ and $S_{\mathrm{CuCu}}(Q)$ in the vicinity of pure Cu:

$$S^{\mathrm{X}}(Q) - w^{\mathrm{X}}_{\mathrm{BiBi}} S_{\mathrm{Bi}}(Q) \approx w^{\mathrm{X}}_{\mathrm{CuCu}} S_{\mathrm{CuCu}}(Q) \qquad (17)$$
$$+ w^{\mathrm{X}}_{\mathrm{BiCu}} S_{\mathrm{BiCu}}(Q)$$

$$S^{\mathrm{n}}(Q) - w^{\mathrm{n}}_{\mathrm{BiBi}} S_{\mathrm{Bi}}(Q) \approx w^{\mathrm{n}}_{\mathrm{CuCu}} S_{\mathrm{CuCu}}(Q) \qquad (18)$$
$$+ w^{\mathrm{n}}_{\mathrm{BiCu}} S_{\mathrm{BiCu}}(Q)$$

This approximation yields severely distorted $S_{\mathrm{BiCu}}(Q)$ partial structure factors. Systematic errors are amplified.

A reverse Monte Carlo simulation [17] was run with a configuration of 2000 atoms. Both structure factors $S^{\mathrm{X}}(Q)$ and $S^{\mathrm{n}}(Q)$ were fitted simultaneously, using the system number density ρ_0 and the closest approach constraints determined from the direct transformation of the total structure factor. Table 1 lists values of the figure of merit R proposed by McGreevy and Pusztai [18] for the relative information content of the two diffraction measurements. R is $1/3$

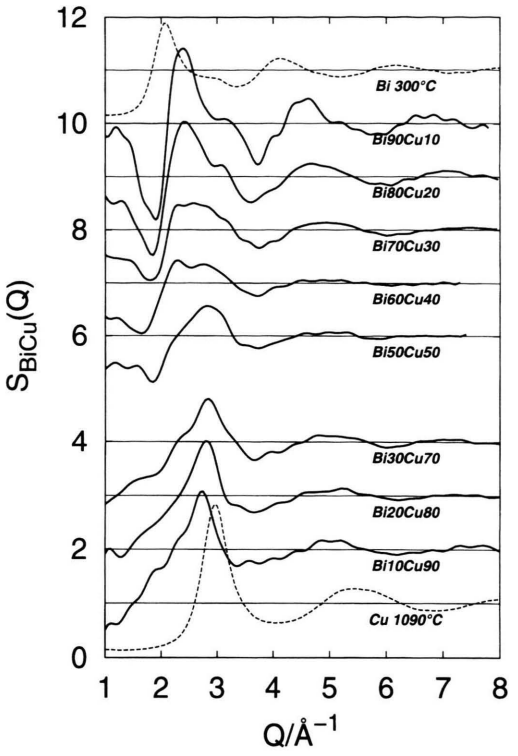

Fig. 10. Assessed partial Bi-Cu structure factors; *full* line: RMC simulation results; *dotted* line: pure elements.

for a single experiment and has a maximum value of 1 when the available experiments directly yield the partial structure factors. The assessment neglects the temperature dependence of the structure factors that is by far less marked than the concentration dependence. The Figs. 8, 9, and 10 show the results for $S_{\mathrm{BiBi}}(Q)$, $S_{\mathrm{CuCu}}(Q)$ and $S_{\mathrm{BiCu}}(Q)$.

5. Discussion

5.1. Pure Elements

The crystal structure of solid Bi is rhombohedral, but Bi becomes more closely packed on melting, with an anomalous density increase. Liquid Bi has a non-simple structure [19]. The first maximum of the Bi structure factor (Fig. 2) is located at $Q_{\max} = 2.05$ Å^{-1}, its height decreases from 1.82 at 300 °C to 1.47 at 900 °C. It is asymmetric: a shoulder on the right hand side located between 2.70 Å^{-1} and 3.20 Å^{-1} is very distinct at 300 °C and slowly disappears at higher temperatures. Although the hard sphere model does not fit this shoulder, a hard sphere diameter of 2.99 Å was found at 700 °C by fitting $S_{\mathrm{Bi}}(Q)$ beyond the first maximum. The first maximum of the Bi pair correlation function $g(r)$ is located at 3.29Å at 475 °C. Its height decreases with temperature, its position changes only slightly.

The crystal structure of solid Cu is face-centred cubic; liquid copper is a simple liquid [20]. The measured structure factor of Cu at 1088 °C shows a symmetrical first maximum at 2.95 Å^{-1} with a height of 2.78 that was fitted using the Percus-Yevick hard core model with a hard sphere diameter of 2.295 Å. A nearest neighbour distance of 2.50 Å was evaluated for this temperature.

5.2. Bi-Cu Structure

On the Bi-rich side of the phase diagram both the neutron and X-ray weight factors for $S_{\mathrm{CuCu}}(Q)$ are very small; $w^{\mathrm{X}}_{\mathrm{CuCu}}$ in Table 1 amounts to only 9% at 55 at.% Cu. Thus, the assessed partial structure factors $S_{\mathrm{CuCu}}(Q)$ are unreliable. The contribution of $S_{\mathrm{BiBi}}(Q)$ dominates the total neutron and X-ray structure factor in this composition range, with the contribution of $S_{\mathrm{BiCu}}(Q)$ growing with the Cu-content. In Fig. 3, a first maximum, virtually like the one in pure Bi at 2.10 Å^{-1}, is predominant, its height decreases slightly from about 1.6 to 1.4 (Figure 11). We therefore assume that $S_{\mathrm{BiBi}}(Q)$ is very similar to the Bi structure factor $S_{\mathrm{Bi}}(Q)$ in this concentration range.

With increasing Cu-content, a subpeak appears on the right-hand side of the main maximum and gradually grows with the mole fraction of Cu. This is ascribed to the growing $S_{\mathrm{BiCu}}(Q)$ contribution. The

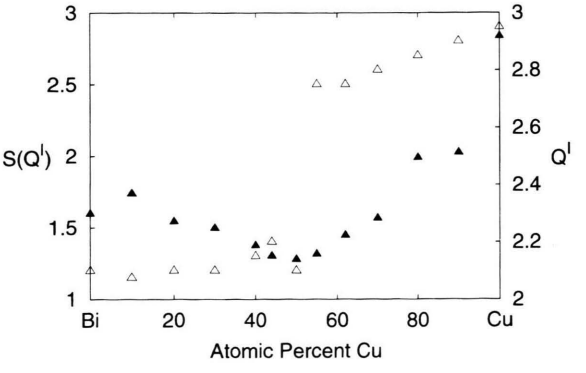

Fig. 11. Concentration dependence of first maximum of Bi-Cu $S(Q)$; *empty* triangle △: Position Q^I of first maximum *filled* triangle ▲: height $S(Q^I)$ of first maximum.

assessed partial structure factor $S_{\mathrm{BiCu}}(Q)$ changes drastically between 10 and 50 at.% Cu.

At 55 at.% Cu, near the inflexion point of the phase diagram, the weight factors $w^{\mathrm{X}}_{\mathrm{BiCu}}$ and $w^{\mathrm{X}}_{\mathrm{CuCu}}$ are alike, the first maximum of $S(Q)$ consists of two subpeaks with nearly the same height. Moreover, $S(Q)$ becomes negative in the low-Q region (near 1 $\mathrm{\AA}^{-1}$). After the first maximum, the total structure factor is strongly damped, with very weak oscillations. The total pair correlation function $g(r)$ shows a shoulder on the left hand side of the first maximum. This shoulder is predominant in the total pair correlation function for neutron scattering, where the contribution of Cu is increased. The model of an additive superposition of the structure factors of the pure elements in Sect. 4.3. is a good fit for $S(Q)$ in this concentration range (Fig. 6), the strong damping after the first maximum is reproduced, since the first maximum of $S_{\mathrm{Cu}}(Q)$ has the same position as the shoulder and the first minimum of $S_{\mathrm{Bi}}(Q)$, whereas the first minimum of $S_{\mathrm{Cu}}(Q)$ coincides with the second maximum of $S_{\mathrm{Bi}}(Q)$. The demixing model infers two distinct nearest neighbour distances in the melt, one for Bi and one for Cu, leading to the strong contrast between X-ray and neutron measurements that is indeed observed at 50 at.% Cu. This suggests that the segregation tendency in the melt is maximum around 50 at.% Cu and matches the small angle scattering results by Zaiss et al. [21]. The negative values of $S(Q)$ mean that the coherently scattered intensity per mean atom $I^{\mathrm{coh}}_{\mathrm{BiCu}}(Q)$ is smaller than the monotonic Laue scattering term $\langle f^2(Q)\rangle - \langle f(Q)\rangle^2$ of a completely random distribution of atoms, which again hints at a microsegregation in the melt.

On the Cu-rich side of the phase diagram from 62 at.% Cu upwards, the contribution of $S_{\mathrm{CuCu}}(Q)$ to the total X-ray structure factor $S(Q)$ becomes remarkable. The main maximum is now located near the maximum of pure Cu, shifted to smaller Q-values. Its height increases with the Cu-content. On the left-hand side of this maximum is a hump whose height decreases with the Cu-content. Its position seems to be shifted to smaller Q-values from the position of the first maximum of pure Bi at 2.10 $\mathrm{\AA}^{-1}$. $S(Q)$ is throughout negative for $Q \approx 1$ $\mathrm{\AA}^{-1}$ except in the close vicinity of pure Cu. It goes through a minimum for $\mathrm{Bi_{30}Cu_{70}}$. A transition occurs in the structure factor of $\mathrm{Cu_{90}Bi_{10}}$ with reference to pure Cu: the height of the maximum is significantly lowered and its position is shifted to smaller Q-values. The $S_{\mathrm{BiCu}}(Q)$ ascendancy by only a few at.% of the larger Bi-atoms suffice to transform the close-packed hard sphere structure of pure Cu into a structure with larger interatomic distances, i. e. a shift of the maximum to smaller Q-values.

6. Conclusion

The behaviour of the Faber-Ziman structure factors of liquid Bi-Cu is qualitatively approximated with a simple demixing model. The splitting of the first maximum of $S(Q)$ into two distinct subpeaks at positions close to those of the maxima of the pure elements is typical for demixing alloy systems with a large difference of the atomic radii. The assessed $S_{\mathrm{BiBi}}(Q)$ is more reliable in the Bi-rich concentration range, where it closely resembles the structure factors of pure Bi. $S_{\mathrm{BiBi}}(Q)$ is less reliable in the Cu-rich range, since both X-ray and neutron weight factors are small. Accordingly, the assessed $S_{\mathrm{CuCu}}(Q)$ is more reliable in the Cu-rich concentration range. This is consistent with the approximation in Section 4.5. The contrast between X-ray and neutron measurements is remarkable and helps to improve the reliability of $S_{\mathrm{BiCu}}(Q)$ in a large concentration range.

Acknowledgements

Financial support from the Bundesministerium für Bildung und Forschung, grant 03-HO5CHE, is gratefully acknowledged.

[1] L.-S. Chang, B. B. Straumal, E. Rabkin, W. Gust, and F. Sommer, J. Phase Equilibria **18**, 128 (1997).
[2] R. N. Singh and F. Sommer, Z. Metallkd. **83**, 533 (1992).
[3] R. V. Gopala Rao and A. Satpathy, Phys. Rev. **B41**, 995 (1990).
[4] W. Zaiss and S. Steeb, Phys. Chem. Liq. **6**, 1 (1976).
[5] Y. Waseda, The Structure of Non-Crystalline Materials, McGraw-Hill, 1980.
[6] W. Hoyer, Promotion B, Diss. 25651, Techn. Universität Karl-Marx-Stadt, 1986.
[7] G. Palinkas, Acta Cryst. **A29**, 10 (1972).
[8] D. Waasmaier and A. Kirfel, Acta Cryst. **A51**, 413 (1995).

[9] S. Brennan and P.L. Cowan, Rev. Sci. Instrum. **63**, 850 (1992).
[10] L. Kissel and R. H. Pratt, Acta Cryst. **A46**, 170 (1990).
[11] T. E. Faber and J. M. Ziman, Phil. Mag. **11**, 153 (1965).
[12] M. Gomez, L. Martin-Garin, H. Ebert, P. Bedon, and P. Desré, Z. Metallkd. **67**, 131 (1976).
[13] S. Frigge, PhD thesis, Diss. 41101, Techn. Universität Chemnitz, 1997.
[14] V. F. Sears, Neutron News **3**, 26 (1992).
[15] O. Akinlade, B. C. Anusionwu, and L. A. Hussain, Z. Metallkd. **89**, 27 (1998).
[16] S. Saadeddine, J. F. Wax, B. Grosdidier, J. G. Gasser, C. Regnaut, and J. M. Dubois, Phys. Chem. Liq. **28**, 221 (1994).
[17] R. L. McGreevy, Nucl. Instrum. and Meth. A **354**, 1 (1995).
[18] R. L. McGreevy and L. Pusztai, J. Neutron Research **3**, 125 (1996).
[19] U. Dahlborg and M. Davidovic, Phys. Chem. Liq. **15**, 243 (1986).
[20] O.J. Eder, E. Erdpresser, B. Kunsch, H. Stiller, and M. Suda, J. Phys. F: Metal Phys. **10**, 183 (1980).
[21] W. Zaiss, S. Steeb, and G. S. Bauer, Phys. Chem. Liq., **6**, 21 (1976).